SURFACE COMPRESSION OF WOUND ROLLS

By

C. Mollamahmutoglu, S. Ganapathi, and J. K. Good
Oklahoma State University
USA

ABSTRACT

Stress levels and profiles in the vicinity of contact between a wound roll and a nip or a rigid surface are important for the quality of the product during manufacturing or storage stages. Excessive or insufficient pressure and stress levels can cause structural damage. This can be crucial for webs that have been recently coated and for all webs that are susceptible of wringing where web layers may fuse or bind together. Herein an efficient computational approach is introduced based on the finite element method for the calculation of stresses in the wound roll which are resulting from contact with a rigid flat surface, a rigid roller or a roller covered with a rubber layer. Compaction experiments carried out on polyester and newsprint webs are used to verify the method. The method accounts for the state dependency of the radial modulus which being affected locally by both winding and contact pressures. It was found that the shear modulus of the stack is important in predicting the contact behavior and had to be determined. The developed numerical tool is used to analyze the stress changes in a wound roll due to contact with a rigid or rubber covered nip roller.

INTRODUCTION

Almost all winding operations are performed in the presence of a nip roller. The nip roller limits the entrainment of air, helps maintain radial uniformity and can increase the wound-on-tension (WOT) in the outer layer of a winding roll. The WOT has components of web tension and nip-induced-tension (NIT). The NIT results from the nip roller inducing slippage in the outer layers of the winding roll. The development of the NIT is affected by contact pressures that result from the nip and complex slip stick behavior of web layers in the nip contact zone [1, 2]. The nip induced stress field is dynamic and travels at the surface velocity of the winding roll. These dynamic stresses superimpose on the roll stresses which result from winding. Rolls that have been wound are stored in a variety of ways. They can be stored supported by their cores or on their ends in stacks but they can also be stored on their edges and furthermore in nested stacks. Rolls supported

on edges will have static non-moving nip stress fields which too will superpose on the residual roll stresses due to winding. Similar static nip stress distributions will result when wound rolls are lifted by clamping their outer surface in preparation for transit. The superposed stress distributions resulting from winding and contact are likely the largest stresses witnessed by the web and thus most likely to damage the web.

Analysis of the superposed stress field is complicated due to the state dependency of the web material properties. An analytical closed form solution based on the classical contact mechanics of the theory of elasticity is intractable [1]. Closed form expressions relating force to deformation are possible if constant average material properties are assumed. Such expressions will not give true insight to the stress fields within the roll which resulted from winding and contact [3,4]. In this case the only viable option is computational tools. The finite element method (FEM) is a robust and powerful solution technique for the analysis of such mechanical problems. Herein a FEM approach for the analysis of the wound roll contact problem will be developed. In finite elements the physical body is divided into sub-domains called 'elements' and governing equations are defined on each of these elements in a discretized manner. These elements will allow the needed spatial variation of the material properties which will be dependent on stresses due to winding and those due to contact [5, 6].

A FINITE ELEMENT MODEL FOR ROLL TO NIP CONTACT

A Practical Mesh Refinement

The contact problem is considered as a 2D plane strain problem. Symmetry about a vertical axis is taken advantage of as shown in Figure 1. Note that vertically only half of each of the wound roll and the nip are modeled. The horizontal boundaries were constrained to have like vertical deformations (v). Since these boundaries were so remote from the contact they were assumed not to affect the solution of the problem due to the principle of St. Venant. The validity of this assumption will be tested later when comparisons are made to laboratory tests. The form of the finite element discretization is shown in Figure 1 with mesh refinement near the contact zone since the deformations, strain and stresses expected to vary rapidly there. An efficient and simple mesh refinement based on a geometric series was employed in both the tangential and radial directions:

$$r_i = (r_{out} - r_{in})\left(\frac{k_r^{i-1} - 1}{k_r^{n_r} - 1}\right)^{p_r} + r_{in}, \quad i = 1,2,..,n_r \qquad \{1\}$$

$$\theta_j = \frac{\pi}{2}\left(\frac{k_\theta^{j-1} - 1}{k_\theta^{n_\theta} - 1}\right)^{p_\theta}, \quad j = 1,2,..,n_\theta \qquad \{2\}$$

Here n_r and n_θ are number of sectors along radial and tangential directions respectively. The parameters k and p are used for controlling the refinement of the mesh in the r and θ directions. Appropriate values will be presented in the results section. r_i and θ_j are the i^{th} radial position and the j^{th} tangential position in cylindrical coordinates. r_{out} and r_{in} are outer and inner radial boundaries of the region which is subjected to refinement. In this case r_{out} and r_{in} can be taken as roll outer radius and core outer radius respectively as we will not refine the core section. An element's radial and tangential position will be used as identification:

$$e_{ID} = (i-1)n_\theta + j, \quad i = 1,2,..,n_r, \quad j = 1,2,..,n_\theta \qquad \{3\}$$

Thus e_{ID} becomes identification number of an element per its radial and tangential location. The coordinates of the refined mesh can be used to define elemental coordinates. This sectored meshing is intrinsically structured and always results in quadrilateral elements. For a generic quadrilateral element, elemental position vector which includes the Cartesian coordinates of 4 nodes can be given as:

$$Q^{e_{ID}} = \left[r_i \cos\theta_j \quad r_i \sin\theta_j \quad r_i \cos\theta_{j+1} \quad r_i \sin\theta_{j+1} \quad r_{i+1} \cos\theta_j \quad r_{i+1} \sin\theta_j \quad r_{i+1} \cos\theta_{j+1} \quad r_{i+1} \sin\theta_{j+1} \right]^T \qquad \{4\}$$

This approach can be applied to the nip roll cylinder when a non-rigid nip roll exists. In the case of a rigid nip there is no need to model the nip roll and nip roll is modeled only by an outer rigid boundary. This will be addressed in the contact algorithm section and in the rubber covered nip roll section.

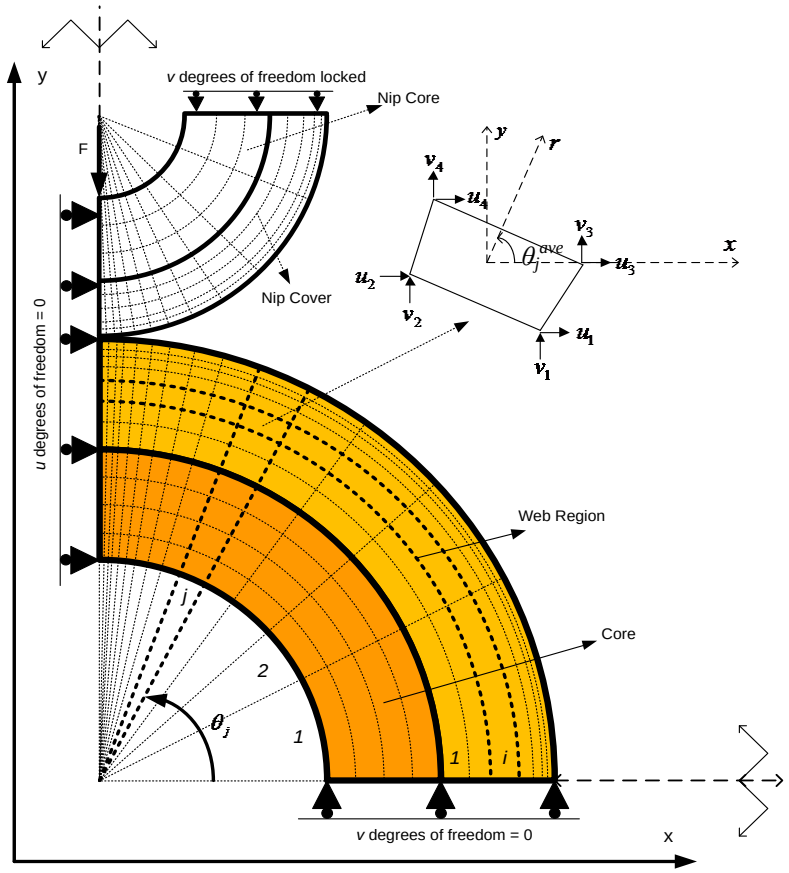

Figure 1 – Finite Element Discretization of Contact Model for Roll and Nip

A Brief Finite Element Formulation

The finite element formulation for this problem will be presented for the sake of completeness. Detailed development is routine and can be found in standard texts [5,6]. A

displacement based finite element formulation results in an element stiffness matrix. The derivation begins with the approximation of continuous displacement field vector *U(x,y)*:

$$U(x,y) = \left[u(x,y) \;\; v(x,y)\right]^T \cong \Phi U^{e_{ID}} \qquad \{5\}$$

$$\Phi = \begin{bmatrix} \phi_1 & 0 & \phi_2 & 0 & \phi_3 & 0 & \phi_4 & 0 \\ 0 & \phi_1 & 0 & \phi_2 & 0 & \phi_3 & 0 & \phi_4 \end{bmatrix}, \;\; U^{e_{ID}} = \begin{bmatrix} u_1 & v_1 & u_2 & v_2 & u_3 & v_3 & u_4 & v_4 \end{bmatrix}^T \qquad \{6\}$$

where *u(x,y), v(x,y)* are displacement fields in the x and y directions respectively, Φ is the shape function matrix for a 4-node quadrilateral element, ϕ_i is the shape function associated with node *i* and $U^{e_{ID}}$ is nodal displacement vector for the element. Components of the displacement vector can be seen in Figure 1. Assuming small deformation theory and employing the usual strain displacement relation, a discretized version for the strain can be obtained:

$$\varepsilon^{e_{ID}} = DU(x,y) \cong (D\Phi)U^{e_{ID}} \qquad \{7\}$$

$$\varepsilon^{e_{ID}} = \begin{bmatrix} \varepsilon_x & \varepsilon_x & \gamma_{xy} \end{bmatrix}^T, \;\; D = \begin{bmatrix} \partial/\partial x & 0 & \partial/\partial y \\ 0 & \partial/\partial y & \partial/\partial x \end{bmatrix}^T \qquad \{8\}$$

where $\varepsilon_x, \varepsilon_y$ and γ_{xy} are the normal strains in the x, y directions and engineering shear strain, respectively. *D* is the differential operator matrix which in this case operates on the shape functions Φ. Now the stiffness matrix $K^{e_{ID}}$ for the element can be given as:

$$K^{e_{ID}} = \int_{V^{e_{ID}}} B^T M^{e_{ID}}_{Cart.} B dV^{e_{ID}} \qquad \{9\}$$

where $B = D\Phi$ is the strain-displacement matrix and $M^{e_{ID}}_{Cart.}$ is the element material matrix in Cartesian coordinates. The material orthotropic behavior of the wound roll is based on cylindrical coordinates which is dictated by the cylindrical body. Material matrices for wound roll elements are given with respect to cylindrical coordinates. For the sake of simplicity the compliance matrix (the inverse of the material matrix) in cylindrical coordinates for plane strain condition is given:

$$C^{e_{ID}}_{Cyl.} = \begin{bmatrix} 1/E_r - v_{rz}^2/E_z & -(v_{r\theta} + v_{rz}v_{z\theta})/E_\theta & 0 \\ -(v_{r\theta} + v_{rz}v_{z\theta})/E_\theta & (E_\theta - E_z v_{z\theta}^2)/E_\theta^2 & 0 \\ 0 & 0 & 1/G_{r\theta} \end{bmatrix} \qquad \{10\}$$

$$M^{e_{ID}}_{Cyl.} = \left(C^{e_{ID}}_{Cyl.}\right)^{-1} \qquad \{11\}$$

where E_r, E_θ, E_z , and $G_{r\theta}$ are the radial, tangential , axial and shear moduli and $v_{r\theta}$, v_{rz} and $v_{z\theta}$ are the Poisson ratios. Now the element material matrix in Cartesian coordinates

can be computed via an orthogonal transformation:

$$M^{e_{ID}}_{Cart.} = R^T M^{e_{ID}}_{Cyl.} R \qquad \{12\}$$

$$R = \begin{bmatrix} \cos^2\theta_j^{ave} & \sin^2\theta_j^{ave} & \sin 2\theta_j^{ave} \\ \sin^2\theta_j^{ave} & \cos^2\theta_j^{ave} & -\sin 2\theta_j^{ave} \\ -\sin 2\theta_j^{ave}/2 & \sin 2\theta_j^{ave}/2 & \cos 2\theta_j^{ave} \end{bmatrix}, \quad \theta_j^{ave} = \left(\theta_j + \theta_{j+1}\right)/2 \qquad \{13\}$$

where R is the orthogonal transformation matrix and θ_j^{ave} is the element's orientation with respect to the x axis. The element stiffness matrix {9} can be numerically calculated for all elements by using a master element concept. Assuming an isoparametric formulation, a transformation of coordinates from the actual (x,y) to natural (η,ξ) coordinates can be carried out:

$$X(x,y) = \left[x(\eta,\xi) \;\; y(\eta,\xi)\right]^T = \Phi Q^{e_{ID}} \qquad \{14\}$$

where X is the position vector, Φ is the shape function matrix used in expression {5} and $Q^{e_{ID}}$ is the elemental position vector defined in {4}. The components of for an isoparametric formulation of a quadrilateral element are:

$$\phi_1 = \frac{(1-\xi)(1-\eta)}{4}, \quad \phi_2 = \frac{(1-\xi)(1+\eta)}{4}, \quad \phi_3 = \frac{(1+\xi)(1-\eta)}{4}, \quad \phi_4 = \frac{(1+\xi)(1+\eta)}{4} \qquad \{15\}$$

Using these shape functions the stiffness integral (per unit thickness) is:

$$K^{e_{ID}} = \int_{-1}^{1}\int_{-1}^{1} \overline{B}^T M^{e_{ID}}_{Cyl.} \overline{B}\,|J|\,d\eta d\xi \qquad \{16\}$$

where $\overline{B} = RB$ and $|J|$ is the determinant of the usual Jacobian matrix J of the transformation X. A 2X2 Gauss quadrature is employed to numerically integrate the stiffness integral {16}. The finite element assembly procedure is used for all elements which results in a total system stiffness matrix for the wound roll shown in Figure 1.

An Efficient and Simple Contact Algorithm

This problem has two kinds of nonlinearity. The first type is material nonlinearity and stems from the known dependence of the radial modulus of elasticity of web materials on pressure or radial stress. One common material model which is often used for webs [7] is:

$$E_r^{e_{ID}} = K_2\left(K_1 - \sigma_r^{-e_{ID}}\right) \qquad \{17\}$$

where $E_r^{e_{ID}}$, $\overline{\sigma}_r^{e_{ID}}$ are radial modulus and average radial stress for the element e_{ID}. K_1 and K_2 are Pfeiffer's material parameters. Prior to contact there is an existing radial stress field, $\overline{\sigma}_r^{e_{ID}} = {}^0\overline{\sigma}_r^{e_{ID}}$, in the wound roll due to winding. A 1D nonlinear winding model, like that of Hakiel [8] but written for plane strain conditions, is employed to determine the stresses and the radial variation of the radial modulus due to winding. This radial

modulus variation is used to set the initial radial modulus ${}^{0}E_r^{e_{ID}}$ for the elements prior to compression by contacts.

The second type of nonlinearity is geometric. This is due to changing contact conditions (geometry) as the compression progresses. In the literature there is vast amount of information on computation of this type of nonlinearity [9]. A common approach is one of linearization using a tangent stiffness formulation based on the Newton-Raphson method. The contact geometry conditions are tracked using complex algorithms which are based on either node-to-node or node-to-surface contact. The current problem deals with the contact of cylinders in compression and involves smooth boundaries with predictable contact patterns. The contact will begin with zero contact force when the tip nodes of the cylinders barely contact as was shown in Figure 1. As the compression progresses the nodes next to the tip node will come into contact sequentially. Thus an efficient and simple quasi-linear approach based on node-to-node contact at the boundaries of the cylinders will be employed. The material nonlinearity in this algorithm will be incorporated in a stepwise approach. In each step an increment in deformation will occur as the compression progresses from one node to the next on the contact surfaces. Element material parameters will be taken as constant during a step deformation and updated at the end of the step. In this manner the system will behave elastically during a step deformation. At the end of each step the total elemental stresses will be updated by the increments in stress that resulted from the step deformation. Then all element material properties dependent on the total radial stress {17} will be updated.

In Figure 2 geometry of contact of two cylinders is shown in detail. When seeking node-to-node contact, the corresponding nodes on the two cylindrical surfaces should be aligned in the lateral direction. Non-slip boundary conditions will be assumed. This will ensure that with increasing compression the lateral deformation of the boundary nodes will be generally smaller than their vertical counterparts, on the order of two magnitudes. By neglecting these small lateral deformations the initially aligned nodes on the two contact surfaces will retain their lateral alignment after a step deformation. Once the mesh refinement is complete for the wound roll this will dictate the lateral locations of the nodes on the boundary of the nip cylinder due to this lateral alignment requirement, as shown in Figure 1. Later this will dictate the mesh structure for the nip roll when a non-rigid nip is employed. Thus the mesh of the nip section will be refined in tangential direction similar to the wound roll. Whether the nip is rigid or not the boundary of the nip will be used to enforce appropriate contact conditions. The logic of the algorithm is quite similar for both cases and only minor modifications are necessary. First, as seen in Figure 2, the initial gap size for the node *i* can be written:

$$\delta_i^0 = r_{out}(1-\sin\alpha_i) + r_{nip}(1-\sin\beta_i), \quad i = 0,1,..,n_{cT} \qquad \{18\}$$

where the angle α_i is directly dictated by the tangential refinement:

$$\alpha_i = \theta_{n_\theta+1-i}$$

The corresponding angle for the nip β_i can be easily calculated due to lateral alignment of the nodes for ensuring node to node contact:

$$\beta_i = \arccos\left(\frac{r_{out}}{r_{nip}}\cos\alpha_i\right) \qquad \{20\}$$

The superscript 0 of the gap size *i*, δ_i^0, in expression {18} indicates the compression step; 0 being the initial, 1 being the case when the node 1 comes in contact and so on. Finally n_{cT} is the total number of nodes with contact potential and is a predefined value. Herein this was set as $n_{cT} = n_\theta/2$.

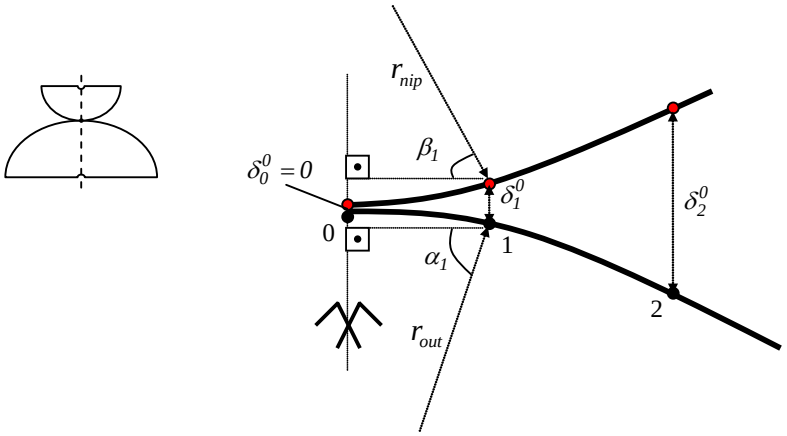

Figure 2 – Initial Geometry of Contact of Two Cylinders

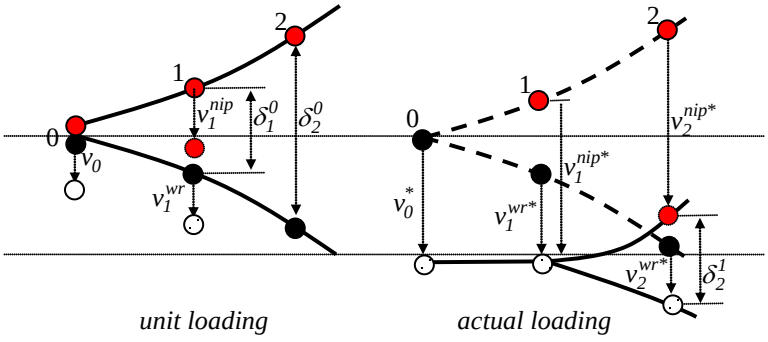

Figure 3 – Deformations During Step 1

The algorithm starts with a unit loading (F=½, due to symmetry) applied at the center of the core of the nip as shown in Figure 1. The system is solved enforcing a set of boundary conditions. The symmetry boundary conditions along the vertical symmetry axis are enforces by setting the *u* degrees of freedom to zero. The wound roll is assumed to be rigidly supported (only the nip is moving) so the *v* degrees of freedom of the nodes along the bottom surface are set to zero. Nodes along the upper edge of the nip roll's quarter cylinder are forced to deform equally in the vertical (v) direction. This is

accomplished using based multi-point constraint (MPC) equations enforced using the penalty approach. In step 1 the contact conditions on the boundary (non-slip, no penetration) begin with node 0 at the boundary of the wound roll and the corresponding node of the nip roll locked together in *x,y* direction. The displacements of the wound roll due to the unit loading are shown in Figure 3 for nodes 0 and 1 as v_0^* and v_1^{wr*}, respectively. Due to the MPC enforced on node 0 the corresponding displacements for the nip are v_0^* and v_1^{nip*}. These displacements will be different from their actual yet unknown counterparts, v_0, v_1^{wr}, v_1^{nip}, which are required to just close the gap at node 1:

$$\delta_1^0 = v_1^{nip} - v_1^{wr} \qquad \{21\}$$

Since linear elasticity is assumed within a step deformation proportionality can be used to estimate deformations other that due to a unit loading:

$$\frac{\Delta F_1/2}{1/2} = \frac{v_1^{wr}}{v_1^{wr*}} = \frac{v_1^{nip}}{v_1^{nip*}} \qquad \{22\}$$

Here ΔF_1 is the unknown actual incremental load which corresponds to actual displacements, again the ½ factor is used in {22} because only half of the system is modeled. Using the geometrical compatibility condition {21} and the proportionality condition {22}, a proportionality parameter κ_1 can be found and used to compute the unknown displacement field and the incremental load ΔF_1 for the entire system for step 1which will just close the gap at node 1:

$$\kappa_1 = \frac{\delta_1^0}{v_1^{nip*} - v_1^{wr*}} \qquad \{23\}$$

$$U_1 = \kappa_1 U_1^*, \quad \Delta F_1 = \kappa_1 \qquad \{24\}$$

Here U_1 and U_1^* are global displacement vectors of the system for actual loading case and unit loading case for step 1. Now the gap sizes for step 2 are updated:

$$\delta_i^1 = \delta_i^0 + v_i^{wr} - v_i^{nip}, \quad i = 2,3,..,n_{cT} \qquad \{25\}$$

The incremental radial stresses for step 1, $\Delta^1\sigma_r^{e_{ID}}$, can be calculated using the step 1 displacements $U_1$and added to the radial stresses due to winding. The updated pressures $\overline{{}^1\sigma_r^{e_{ID}}}$ are the used to recalculate the radial modulus of the elements ${}^1E_r^{e_{ID}}$ for step1:

$$\overline{{}^1\sigma_r^{e_{ID}}} = \overline{{}^0\sigma_r^{e_{ID}}} + \Delta\overline{{}^1\sigma_r^{e_{ID}}}, \quad {}^1E_r^{e_{ID}} = K_2\left(K_1 - \overline{{}^1\sigma_r^{e_{ID}}}\right) \qquad \{26\}$$

This completes step 1. The same procedure is applied for steps 2,3,..,s with applying MPC for boundary node sets *(0,1),(0,1,2),..,(0,1,..,s-1)* respectively until a total load after step *s* is reached:

$$\sum_{i=1}^{s} \Delta F_i \geq F_{nip} \qquad \{27\}$$

Here F_{nip} (units force/width) is the total user defined nip load. The complete generalized algorithm is presented in Table 1.

#	Description
1	Use Hakiel's model to obtain initial stresses due to winding only.
2	Generate refined mesh structure, extract initial values of pressures from Hakiel's model and compute initial radial modulus $^{0}E_r^{e_{ID}} = K_2(K_1 - \overline{^{0}\sigma_r}^{e_{ID}})$
3	set step number $s=1$,calculate initial gap sizes $\delta_i^0 = r_{out}(1-\sin\alpha_i) + r_{nip}(1-\sin\beta_i)$, $i=0,1,..,n_{cT}$
4	Form system stiffness matrix for step s and apply boundary conditions via penalty method $K_s = K_s(\,^{s-1}E_r^{e_{ID}})$
5	Apply MPC contact conditions for step s for boundary nodes $i=0$ to $s-1$
6	Solve constrained system for unit vertical loading at the center of the inner boundary of the core of the nip and obtain corresponding displacements U_s^*
7	Using geometrical compatibility and elastic proportionality calculate proportionality factor for step s $\kappa_s = \dfrac{\delta_s^{s-1}}{v_s^{nip*} - v_s^{wr*}}$
8	Obtain actual incremental compression force and deformations for step s and calculate incremental stresses $\Delta F_s = \kappa_s, U_s = \kappa_s U_s^*$
9	Update gap sizes, total pressures and recalculate pressure dependent radial modulus of elements $\delta_i^s = \delta_i^{s-1} + v_i^{wr} - v_i^{nip}$, $i=s+1$ to n_{cT} $\overline{^{s}\sigma_r}^{e_{ID}} = \overline{^{s-1}\sigma_r}^{e_{ID}} + \Delta\overline{^{s}\sigma_r}^{e_{ID}}$, $^{s}E_r^{e_{ID}} = K_2(K_1 - \overline{^{s}\sigma_r}^{e_{ID}})$
10	Check if target nip force is achieved or not: $\sum_{i=1}^{s} \Delta F_i \geq F_{nip}$ If yes, stop and print results, otherwise $s=s+1$ and go to 4

Table 1 – Compression Algorithm

NUMERICAL RESULTS AND EXPERIMENTAL VERIFICATION

Compression between Rigid Platens and Determination of Shear Modulus

The first application will be to study the load versus deformation of a wound roll between flat, rigid platens. Both 51 μm (200 gage) polyester (PET) film and an 88 μm (350 gage) newsprint paper were used in the experiments. The material data is given in Table 2. These webs were wound with various tension levels and then compressed across their diameters between two rigid platens in an Instron 8502 servo-hydraulic testing system. The experimental setup can be seen in Figure 4. The roll weights were comparable to the nip load levels and a counterbalance is used to eliminate the dead weight of the rolls. Thus the compression of the wound roll due to forces imposed by the testing system alone could be studied. As indicated in the algorithm, the initial stresses and radial modulus at the completion of winding must be computed. During winding, pull tabs were inserted to verify the initial stresses computed from the winding code. The pull tabs were dislodged using a force gage from which the contact pressure could be estimated. In this context pressure levels were measured inside wound rolls of PET film wound at two tension levels (T_w=*6.9* and *4.6* MPa) . Figure 5 shows the radial pressures ($-\sigma_r$) with pull tab results and good agreement is seen. Similar agreement was found for the rolls wound using newsprint.

Material	PET	Newsprint	Geometrical	PET	Newsprint
K_1*(KPa)*	7.24	0.145	web thickness (mm)	0.051	0.089
K_2	40.86	38.4	roll width (cm)	15.24	15.24
E_θ*(MPa)*	4900	3896	roll inner radius (cm)	4.29	4.29
E_z*(MPa)*	4900	3896	roll outer radius (cm)	11.99	11.99
$v_{r\theta}$, v_{rz}	0.01	0.01	core inner radius (cm)	3.81	3.81
$v_{\theta z}$	0.3	0.3	n_r, n_θ	40	40
E_c*(GPa)*	200	200	k_r, k_θ	0.95	0.95
v_c	0.3	0.3	p_r, p_θ	0.5	0.5

Table 2 – Material and Geometrical Data for PET and Newsprint

Before proceeding to compression model a relation for the shear modulus $G_{r\theta}$ is needed. Although not significant on the stresses due to winding only, $G_{r\theta}$ was found to significantly affect the results of the compression model. There is no information in the literature on the prediction or measurement of this value for stacks of web material. It is generally accepted that $G_{r\theta}$ is an independent constant for orthotropic materials. However for bulk orthotropic materials two relations were found, Szilard [10] and Cheng [11]:

$$G_{r\theta}^{Szilard} = \frac{\sqrt{E_r E_\theta}}{2\left(1+\sqrt{v_{r\theta} v_{\theta r}}\right)} \quad \{28\}$$

$$G_{r\theta}^{Cheng} = \frac{E_r E_\theta}{E_r\left(1+v_{\theta r}\right)+E_\theta\left(1+v_{r\theta}\right)} \quad \{29\}$$

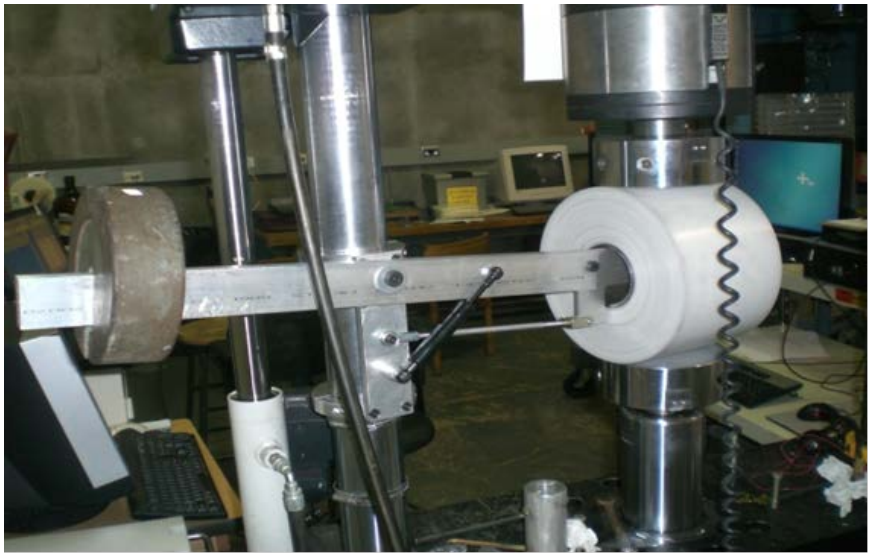

Figure 4 – Experimental Compression Setup

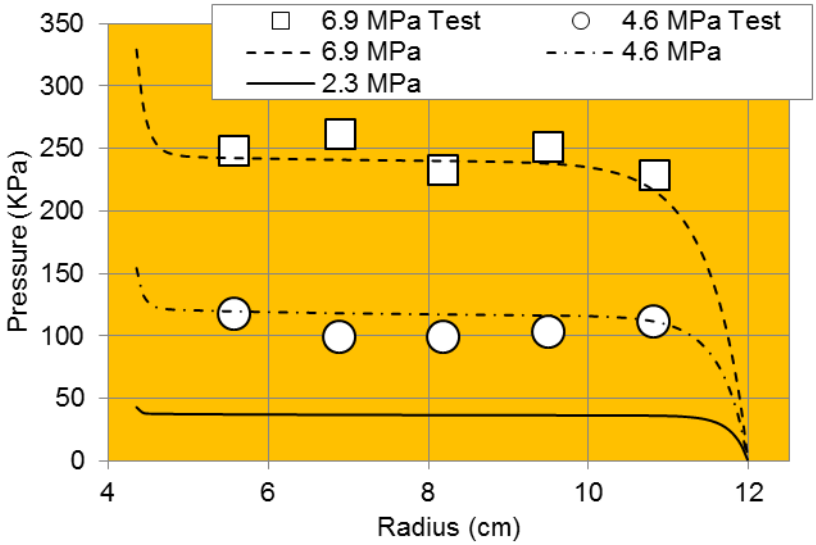

Figure 5 – 200 Gage PET Winding Pressures

In most web materials the out-of-plane Poisson's ratios are small when compared to unity ($\nu_{r\theta}, \nu_{\theta r} << 1$). Moreover the tangential material modulus is far greater than the radial material modulus ($E_\theta >> E_r$). Thus the expressions of Szilard {28} and Cheng {29} would reduce to the following expressions:

$$G_{r\theta}^{Szilard} \approx \frac{\sqrt{E_r E_\theta}}{2} \qquad \{30\}$$

$$G_{r\theta}^{Cheng} \approx E_r \qquad \{31\}$$

Both cases involve the radial modulus E_r thus the shear modulus directly becomes pressure dependent as well. In Figure 6 load-deformation curves are given for the PET film wound with T_w=4.6 MPa. The compression model produces quite different curves with the original forms of shear modulus {30} and {31} but if two times the value of the shear modulus due to Cheng ($G_{r\theta} = 2G_{r\theta}^{Cheng} \approx 2E_r$) is used good agreement with the experimental data was obtained. In order to confirm this finding the expression $G_{r\theta} = 2E_r$ was tested for other winding tension levels and on newsprint. In Figures 7 and 8 curves of load versus deformation are shown for various winding tensions levels for rolls wound from the PET film and Newsprint. The compression model with $G_{r\theta} = 2E_r$ assumption agrees well for all cases. Thus this combined procedure (experiment and numerical model) verifies the use of this relation for two very different materials under various winding conditions.

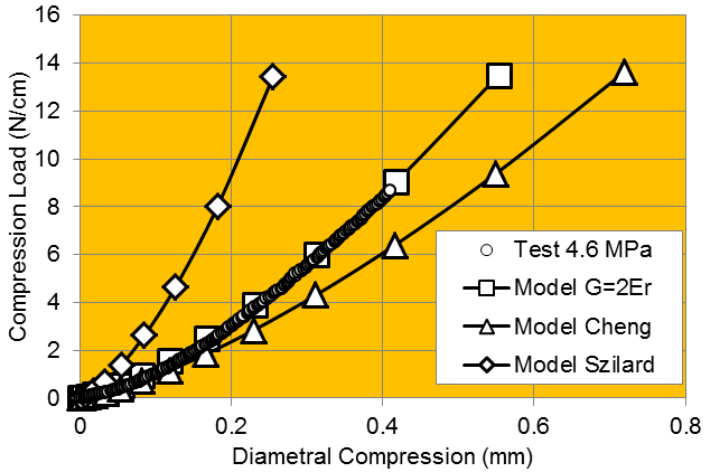

Figure 6 – Comparison of Shear Modulus Expressions

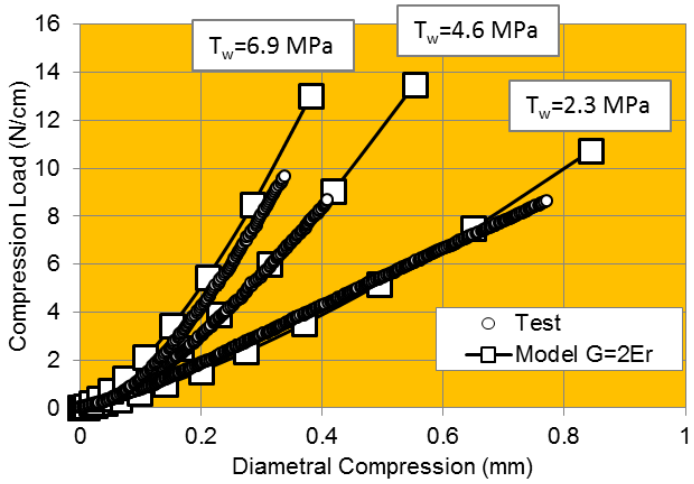

Figure 7 – Model and Test Comparisons for PET

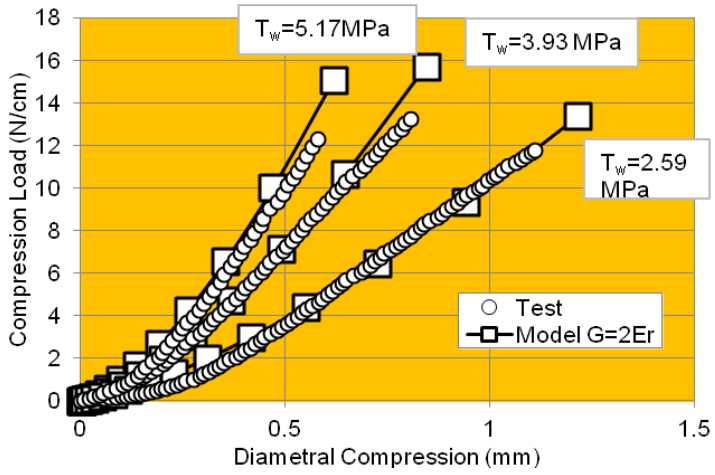

Figure 8 – Model and Test Comparisons for Newsprint

Modeling of Rubber Covered Rollers

In many winding applications nip rollers are covered with a deformable layer. One of the most common materials used for roll covers is rubber. In general rubber is known for its complexity in modeling. There are numerous studies in the literature which aim to model the rubber under various conditions [12]. The theoretical background of these models is mainly based on hyper-elasticity. The determination of the coefficients of these hyper-elastic models usually requires extensive testing on samples which is a complicated task in the field. Thus, especially in web applications, engineers dealing with rubber covered rollers often employ less sophisticated characterization methods. Rubber is often characterized by hardness measurement. A common hardness measurement is the Shore A (i.e. IRHD) hardness which is easily measured with a hand-held instrument in the field. In this study the Shore A (or IRHD) hardness will be used to characterize the rubber properties. This was adopted from an earlier work that modeled the nip contact

between rubber covered nip rollers in contact with other rubber covered and uncovered rollers [3]. One portion of this study was extensive compression tests in which the modulus of elasticity (E_{rubber}) and Poisson's ratio (ν_{rubber}) were measured for various rubber types (carboxilated nitrile, ethylene propylene, hypalon, natural, neoprene, nitrile, and urethane) and varied hardness levels. An exponential expression was found to fit the modulus for all rubber types nicely as a function of hardness (IRHD) alone:

$$E_{rubber} = 0.1446e^{0.0564*IRHD}(MPa) \qquad \{32\}$$

The experimental values for Poisson's ratio for various rubbers yielded an average value of 0.459 which is well beyond the compressibility limits ($\nu<0.4$). The almost incompressible behavior of rubber is a well-known phenomenon which complicates the modeling with displacement based finite elements. Briefly, as the Poisson's ratio approaches to the 0.5 limit the bulk modulus approaches to infinity and the volumetric strain approaches zero. Calculation of the tiny volumetric strains accurately requires intensive mesh refinement. Even so the pressures which are calculated from the displacements can have a large error margin since they are not the primary solution variables of a displacement formulation. This phenomenon is called 'locking' in the finite element formulations. In the literature there are various techniques in order to deal with this problem [5]. One such technique is introducing pressures and displacements as separate unknown independent variables in the formulation. In this manner these types of 'mixed' formulations approximate the unknown pressures directly hence for a same finite element mesh they are much accurate compared with a pure displacement formulation. The cost is a more complicated algorithm and a larger system matrix due to additional pressure unknowns. In this study displacement based elements for the modeling of nip cover were employed. This is justified by using a very fine mesh near the contact zone for the cover and thus the displacements of the rubber cover will be adequately calculated for updating the contact conditions. Also this study is concerned with the pressures inside the wound roll section so the accuracy of the pressures inside the rubber cover is of secondary importance.

As a verification of the selected rubber model the compression model developed herein was used to study the contact of rubber covered rollers in contact with identical rubber covered rollers or with metal (comparatively rigid) rollers for which test data existed [3,14]. In Figure 9, Figure 10 and Figure 11, the experimental load-deformation data for the compression of various rubber covered rollers under low, medium and high nip loads are presented, respectively. For further comparison, a hyper-elastic solution was included which was obtained using commercial finite element software (ABAQUS). The ABAQUS solution is based on the simplest hyper-elastic model which is a Neo-Hookean material model. There are two coefficients (C_{10} and D_1) needed to define a Neo-Hookean material. For small deformations these coefficients can be easily calculated from Young's modulus and Poisson's ratio:

$$\begin{aligned} C_{10} &= G/2 \\ D_1 &= 2/\kappa \end{aligned} \qquad \{33\}$$

where G is the shear modulus ($E/(2(1+\nu))$) and κ is the bulk modulus ($\kappa = E/(3(1-2\nu))$). In the ABAQUS solution a very fine mesh, advanced contact algorithms, a nonlinear geometric formulation and so 'mixed formulation' type elements

(CPE4IH) which are specifically formulated for nearly incompressible materials were employed. The material and geometric data for the rubber covered and metal (rigid) rollers are given in Table 3. Figure 9 and Figure 10 shows results for the compression of identical rubber covered rollers whereas Figure 11 shows results for compression of the rubber covered roller with a metal (rigid) roller. Hence axis labels of Figure 9 and 11 indicate 'radial compression' (total deformation divided by two) whereas the axis label of Figure 10 indicates 'radial penetration' (indentation depth of the rigid roll inside a stationary rubber covered roll). From Figures 9, 10 and 11 compression model solutions almost duplicate the ABAQUS solutions and compare nicely with the test data. This shows the effectiveness of the algorithm presented here as it is able to produce excellent results for a broad range of loading levels and hardness levels. This also shows the effectiveness of the IRHD characterization of Young's modulus for rubber materials.

Roller	IRHD	E (MPa)	ν	Diameter (mm)	Cover Thickness (mm)
L_1	76	10.51	0.458	62.7	5.1
L_2	60	4.26	0.458	165.1	7.5
L_3	61	4.51	0.458	127	12.7
M_1	57	3.60	0.458	152.7	3.3
M_2	52	2.72	0.458	152.1	4.4
M_3	45	1.83	0.458	152.2	12.7
H_1	62	4.77	0.458	76.6	12.7
H_2	46	1.94	0.458	76.6	12.7
H_3	30	0.79	0.458	76.6	12.7
M_R	-	-	-	152.4	-

Table 3 – Material and Geometrical Data for Rubber Covered Rollers

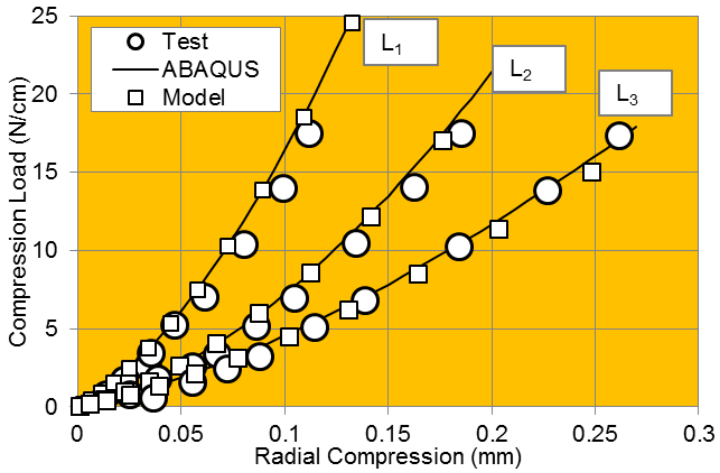

Figure 9 – Model and Test Comparisons for Rubber Covered Rollers – Low Nip Load Levels.

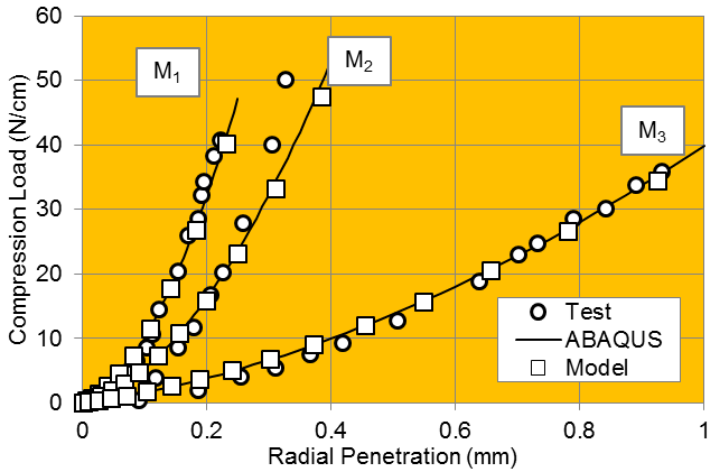

Figure 10 – Model and Test Comparisons for Rubber Covered Rollers – Medium Nip Load Levels.

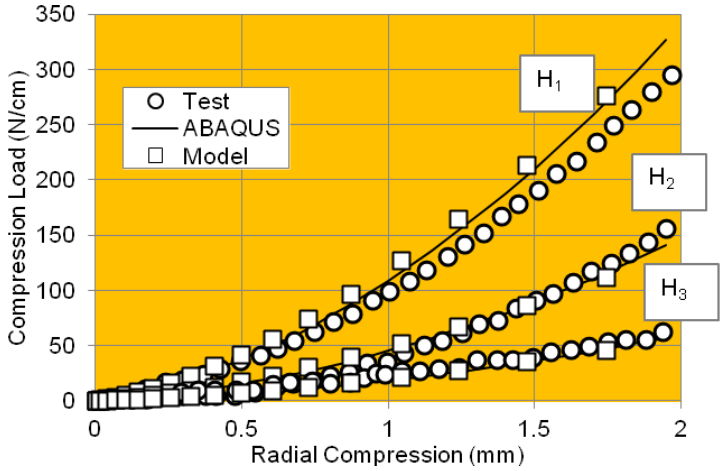

Figure 11 – Model and Test Comparisons for Rubber Covered Rollers – High Nip Load Levels.

Some Compression Scenarios and Altered Stress States

In this section the stress state alterations inside the wound rolls due to compression exerted by various rollers will be examined. The scenarios include compression of a wound roll by a hard (IRHD 80) and soft (IRHD 40) rubber covered rollers, a rigid roller and finally compression due to dead-weight (wound roll resting on a rigid flat surface). The material and geometric data for the rollers are given in Table 4. The selected web material is the polyester film which was defined in Table 2 and previously used in the diametral compression tests. In this case the PET film was wound with a tension level of 3.45 MPa. The applied nip load is same for all scenarios and it is equal to the dead weight loading (≈36 N/cm) if an average value of 1.4 g/cm^3 is taken for the density of the polyester. Since the algorithm is of the displacement control type the solution completes

once the load level exceeds the predefined value. Thus the final load level differs from one scenario to another yet they are close to each other and greater than the predefined value of 36 N/cm. If one wants to model the load levels with higher accuracy simply increase the number of elements along tangential direction on the boundary. This will increase the load level resolution.

	Rigid Surface	Rigid Roller	Soft Rubber Covered	
IRHD	-		40	80
cover thickness (cm)	-		1.27	
roller diameter (cm)	40.64			
roll in. diameter (cm)	8.38			
roll out. diameter (cm)	60.96			
roll width (cm)	60.96			
T_w (MPa)	3.45			
nip load (N/cm)	40			

Table 4 – Material and Geometrical Data for Compression Scenarios

In Figure 12 the surface pressures with respect to half contact width are shown. As expected the rigid roller produced the highest pressure levels with the minimum contact width. The soft rubber covered roller produced the lowest pressure levels with the maximum contact width. As the rubber becomes very hard (IRHD $\rightarrow$100) the rubber covered roller will behave as a rigid material when compared to roll wound of PET film. In Figure 13 the in-roll radial pressures beneath contact zone are shown. It is seen that significant increases in the total radial pressures are experienced towards surface of the roll where the contact occurs. The maximum surface contact induced pressures in Figure 12 are very close to surface pressures of Figure 13 per mechanical equilibrium. In Figure 13 the radial pressure may be observed to rapidly diminish away from the contact surface and winding induced pressures dominate when radius is smaller than 25 cm. This boundary is also matching with the boundary of the pressure plateau. Thus it can be concluded that the most effected part is the relatively soft outer part of the wound roll which comes after the almost constant pressure plateau due to constant tension winding. The maximum pressures here are almost 2 to 3 times of the plateau region and far greater than the maximum stresses near core (≈100 KPa).

The tangential stresses were found to be strongly dependent on friction modeling of contact. As indicated earlier rough contact was assumed and no slippage was permitted. The average tangential stresses beneath contact region (around radius 30.45 cm) are shown in Figure 14 with respect to applied nip load. Significant drops in tangential stress are witnessed due to compaction. Note that rubber covers caused greater compaction than the rigid surfaces under these contact conditions.

Model Limitations

The proposed model has two limitations. The first limitation regards very large deformations. The contact conditions are updated with geometry changes and the model predicts deformations nicely, even at high nip loads. For extreme cases the circular geometry of the wound roll will become elliptical. Also for extremely soft rubber covers the contact algorithm does not model the contact well due to large deformations within the rubber cover.

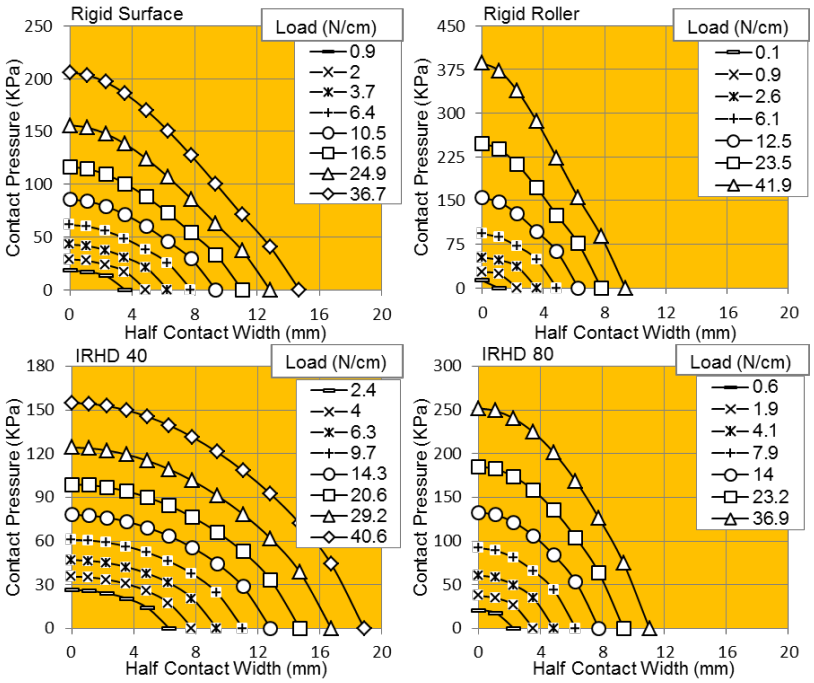

Figure 12 – Surface Contact Pressures vs. Contact Width.

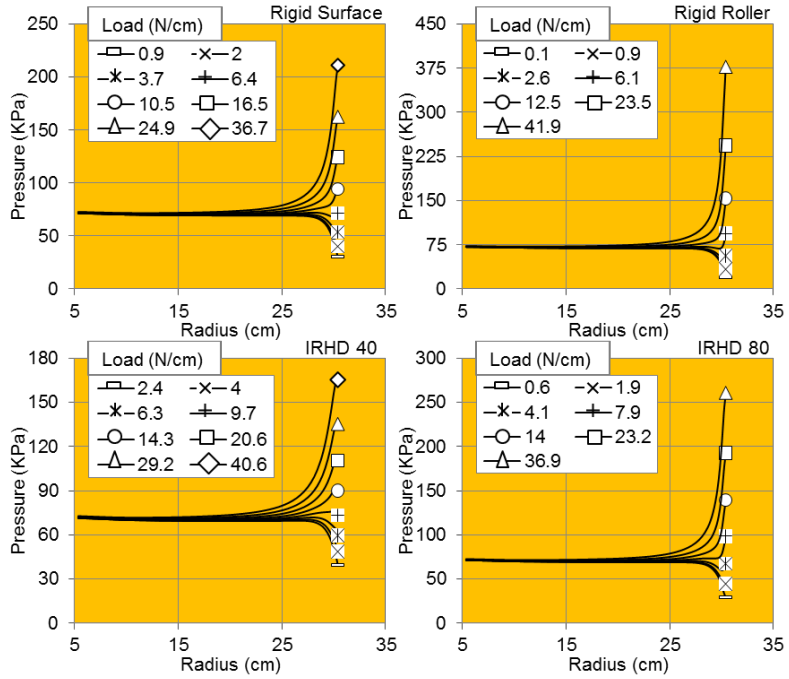

Figure 13 – Radial Pressure Changes in the Roll

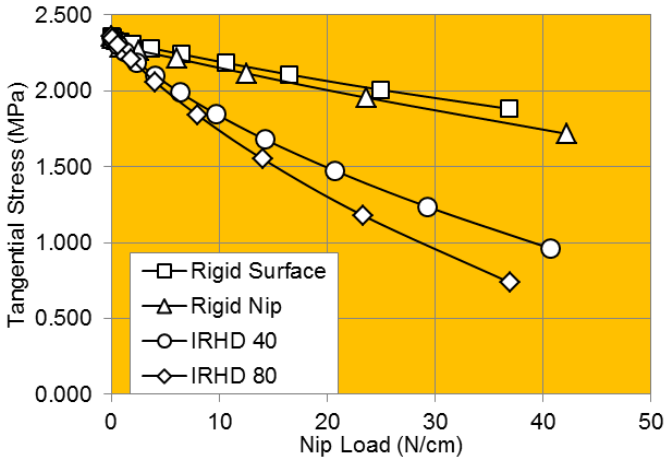

Figure 14 – Average Tangential Stress Changes beneath Contact Zone

Geometric large deformation effects will play an important role in these situations and the model does not take into account such effects. The second limitation is somewhat related with the first one: The model does not take into account any separation or slippage of layers due to excessive nip load or loose winding conditions. The model assumes the wound roll as a continuum than a layered structure. The model size is much reduced by not accounting for slippage or separation between layers. The model ignores any slippage and separation due to excessive shear stresses and tensile stresses which might develop between the layers. Low winding tensions combined with excessive nip load can induce these behaviors. In Figure 15 load versus deformation results for the compression of the newsprint wound roll between rigid platens are shown. This roll was wound at a lower winding tension (T_w =1.29 MPa). The good agreement seen earlier in Figure 8 is not witnessed here. A decrease in stiffness is observed as compression increase and is a clear manifestation of loss of structural integrity. Contour plots for radial pressure, shear stress, tangential stress and slip factor for this case are shown in Figure 16. The slip factor is the ratio of the shear stress to shear restraining capacity (pressure multiplied by the coefficient of friction μ) per a Coulomb friction model . It is evident that shear slippage is occurring during compression. Another interesting result is development of positive tangential stresses in the mid region along the symmetry axis of roll. This is also an arching behavior observed in the tangential stresses.

CONCLUSIONS

The model developed herein can be used to address the stress state of a compressed roll under its own weight or in contact with a rigid or a rubber covered roller. Significant pressures were shown to develop in the contact zone. As expected, at a fixed contact load level the harder impinging roller with smaller roll radius will produce higher contact pressure. Significant pressures can develop in a roll due to its own weight. Relatively loose rolls (wound with low web tension) may be susceptible to structural integrity problems due to slippage and/or separation of layers under high load. Compression tests can be run on webs to determine what levels of contact pressure will damage the web. This model can then be used to determine how large a nip load can be or how large the dead weight of a roll in contact with a storage surface can be without causing damage.

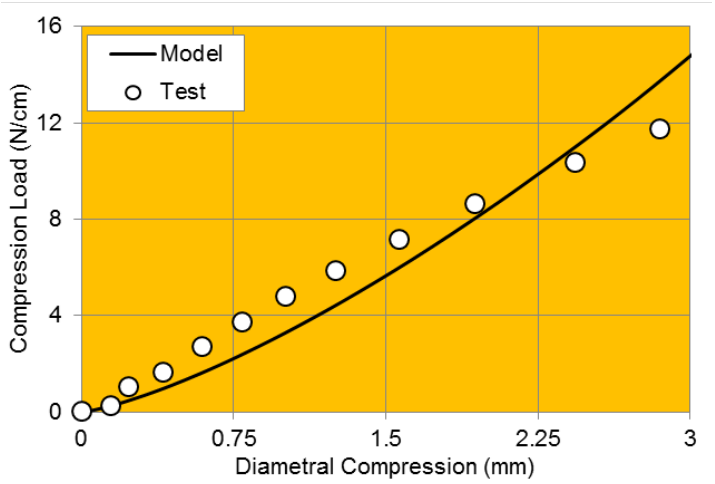

Figure 15 – Model and Test Comparisons for Newsprint Roll Wound with T_w=1.29 MPa. Compression Load = 15 N/cm.

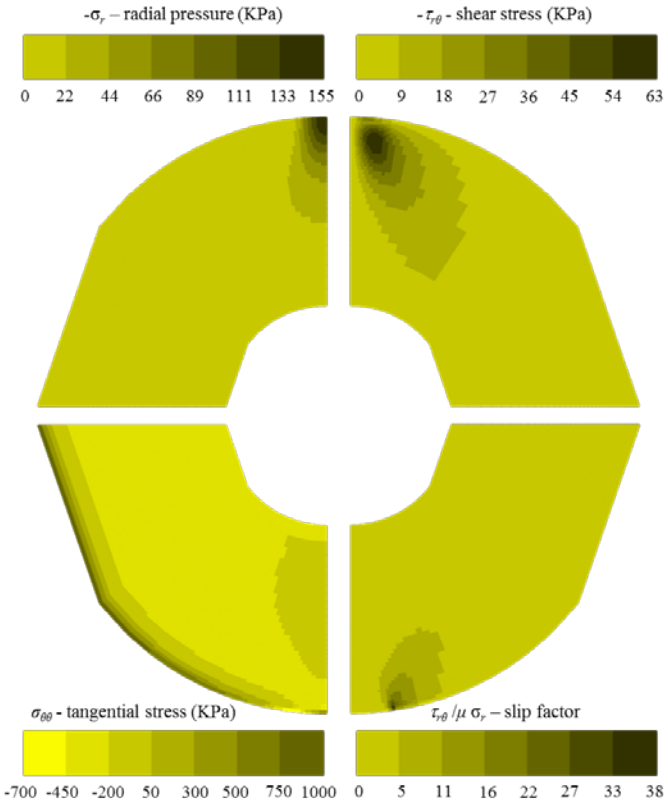

Figure 16 – Pressure, Shear Stress, Tangential Stress and Slip Factor Contours for Newsprint Roll Wound with T_w=1.29 MPa Compression Load = 15 N/cm μ=0.3 [13].

One of the indirect but important findings of the model is the prediction of the relation between radial modulus and shear modulus. Prior to this study there was no source in the literature which addressed the shear modulus of wound rolls. This study has methodically (combined experiments and numerical model) proven that $G_{r\theta} = 2E_r$ applies for two very different web materials (Newsprint and PET) under varied winding conditions. Another indirect result from this study was the additional verification of IRHD based modeling of rubber covered rollers and the computational savings this provided the contact model. Rubber covered rollers in compression were well modeled based on hardness. This simple method of characterization of rubber may well have other applications in the web handling industry.

ACKNOWLEDGEMENTS

The authors would like to acknowledge the sponsors of the Web Handling Research Center of Oklahoma State University for the support they provided which allowed us to pursue the research reported herein.

REFERENCES

1. Kandadai, B.K. and Good, J.K., "Winding Virtual Rolls," Tappi Journal, Vol.10, Issue 6, 2011, pp. 25-31.
2. Kandadai, B.K., Good, J.K., and Markum, R., "A New Method for Measurement of Wound-in-Tension in Webs Wound into Rolls," Journal of Pulp and Paper Science, Vol. 35, Issue 1, 2009, pp. 17-23.
3. Good, J.K., "Modeling Rubber Covered Nip Rollers In Web Lines," Proceedings of the Sixth International Conference on Web Handling, June 2001, Oklahoma State University, pp. 159-186.
4. Johnson, K.L., Contact Mechanics, Cambridge University Press, 1989, pp. 139-140.
5. Bathe, K.J., Finite Element Procedures, Prentice Hall, 1996, pp. 485.
6. Reddy, J.N., An Introduction To The Finite Element Method, McGraw-Hill, 2006, pp. 607.
7. Pfeiffer, J.D., "Internal Pressures in a Wound Roll of Paper," Tappi Journal, 1966, Vol. 49, pp. 342-347.
8. Hakiel, Z., "Nonlinear Model for Wound Roll Stresses," Tappi Journal, 1987, Vol. 70, No. 5, pp. 113-117.
10. Szilard, R., Theory and Analysis of Plates, Prentice Hall, 1974, pp. 375-376.
11. Cheng, S. and Cheng, C.C., "Relation between E, ν, and G and Invariants of the Elastic Coefficients for an Orthotropic Body," Mechanics of Wood and Paper Materials, American Society of Mechanical Engineers, AMD-Vol. 112, MD-Vol. 23, 1990, pp. 63-65.
12. MSC Software: "White Paper – Nonlinear Finite Element Analysis of Elastomers"
13. McDonald, J.D. et. al., "Measuring Paper Friction: Testing Conditions and Papermaking Factors," Tappi Finishing and Converting Conference, 1996, pp. 161-171.
14. Miller, R.D.W., "Variations of Line Pressure and Rolling Speed with Indentation of Covered Rollers," British Journal of Applied Physics, Vol. 15, 1964, pp.1423-1435.